Lattice dynamics of the cluster chain compounds $M_2Mo_6Se_6$ (M = K, Rb, Cs, In, and Tl)

Liam Gannon,[1,2] Lilia Boeri,[3] Christopher A. Howard,[4] Patrick Gougeon,[5] Philippe Gall,[5] Michel Potel,[5] Diala Salloum,[5,*] Alexander P. Petrović,[6,†] and Moritz Hoesch[1,7,‡]

[1]*Diamond Light Source, Harwell Campus, Didcot OX11 0DE, United Kingdom*
[2]*Clarendon Laboratory, University of Oxford Physics Department, Parks Road, Oxford, OX1 3PU, United Kingdom*
[3]*Dipartimento di Fisica, Sapienza Università di Roma and Istituto dei Sistemi Complessi, ISC-CNR, 00185 Rome, Italy*
[4]*Department of Physics & Astronomy, University College London, London WC1E 6BT, United Kingdom*
[5]*Laboratoire de Chimie du Solide et Inorganique Moléculaire, UMR CNRS 6226 - INSA, Université de Rennes 1, Avenue du Général Leclerc, 35042 Rennes-Cedex, France*
[6]*Department of Quantum Matter Physics, University of Geneva, 24 Quai Ernest-Ansermet, 1211 Geneva, Switzerland*
[7]*DESY Photon Science, Deutsches Elektronen-Synchrotron, Notekestrasse 85, 22607 Hamburg, Germany*

(Received 31 March 2018; revised manuscript received 19 June 2018; published 9 July 2018)

The lattice dynamics of members of the $M_2Mo_6Se_6$ family of materials with guest ions M = K, Rb, Cs, In, and Tl has been studied using inelastic x-ray scattering and Raman spectroscopy at room temperature, as well as by *ab initio* calculations. We find a good match between calculations and experiment, both for structure factors (eigenvectors) and for the calculated phonon frequencies. The observed lattice dynamics for $Tl_2Mo_6Se_6$ show no signs of anharmonicity or absence of avoided dispersion crossings, thus ruling out previously hypothesized rattling phonon modes. The reduced mode energies for $In_2Mo_6Se_6$ are identified as only partially responsible for the lower superconducting transition temperature T_c in this material when compared to $Tl_2Mo_6Se_6$.

DOI: 10.1103/PhysRevB.98.014104

I. INTRODUCTION

Materials with uniaxial anisotropy of the crystal lattice are of interest for the research on one-dimensional electronic systems that could form if the charge carriers were confined to motion along individual chains of atoms, molecules, or clusters. The electronic structure of real materials will include a finite interchain coupling, but it is still justified to speak of a quasi-one-dimensional (q1D) state if the hopping along chains is much easier than between chains. Many materials have been identified as having a suitable chain arrangement in their crystal structure [1]. These materials thus allow the study of the intriguing and well-established theoretical predictions, in particular if the band filling allows for a metallic state [2]. One-dimensional confinement of the electrons occurs in materials that still feature three-dimensional long-range order and, apart from strong mechanical anisotropies [3,4], have regular vibrational properties.

The family of compounds $M_2Mo_6Se_6$ derives from Mo_3Se_3 cluster units that are stacked along the c axis of a hexagonal lattice with two cluster units per unit cell as shown in Fig. 1 [5,6]. M guest ions that can be alkali metals (Na, K, Rb, Cs) or group III metals (In or Tl) occupy highly symmetric positions between the chains. Owing to the winding arrangement of Mo_3 triangles that are rotated by 60° from cluster to cluster the chains are sometimes referred to as nanotubes. A single electronic band leads to metallic conductivity. This band, derived from Mo 4*d* states that are delocalized over the clusters, has a chiral wave function as identified by density-functional-theory calculations [7]. The interchain coupling increases along the group of alkali metals from Rb to Na and is significantly higher for $In_2Mo_6Se_6$ and $Tl_2Mo_6Se_6$ [8]. This chiral electron band was later described as an electron band of cubic Dirac fermion type by considering all symmetries of the $P6_3/m$ space group [9,10], which was subsequently discussed in terms of topological superconductivity [11].

Strongly anisotropic superconductivity (SC) has been observed in all family members, which is remarkable given the highly q1D electronic system that renders the SC unconventional. In $Tl_2Mo_6Se_6$ this has been consistently observed ever since the first samples were synthesized [12]. The highest observed transition temperatures are up to $T_c = 5.8$ K in $Tl_2Mo_6Se_6$ (onset at 6.8 K) [12] and $T_c = 2.85$ K in $In_2Mo_6Se_6$ [7]. This SC is likely to be phonon mediated and remarkable thermoelectric properties relate to electron phonon coupling (EPC) as well [13–15]. Due to the high temperatures required for synthesis and single crystal growth the samples sometimes have significant amounts of vacancies in the guest ion positions, while the (Mo_3Se_3) cluster chains have extremely low defect densities. The stoichiometry can deviate from the ideal $M_2Mo_6Se_6$ as much as $M_{1.7}Mo_6Se_6$ for lighter M ions [8,16]. Alkali metal family members show a broad minimum of resistivity with a minimum at temperatures that increase with increasing disorder [8]. Careful experiments have found SC also in the high-resistance low-temperature state and this was related to localization effects [8,17]. A dimensional crossover

*Permanent address: Faculty of Science III, Lebanese University, PO Box 826, Kobbeh-Tripoli, Lebanon.
†Present address: Division of Physics and Applied Physics, School of Physical and Mathematical Sciences, Nanyang Technological University, 21 Nanyang Link, Singapore 637371.
‡moritz.hoesch@desy.de

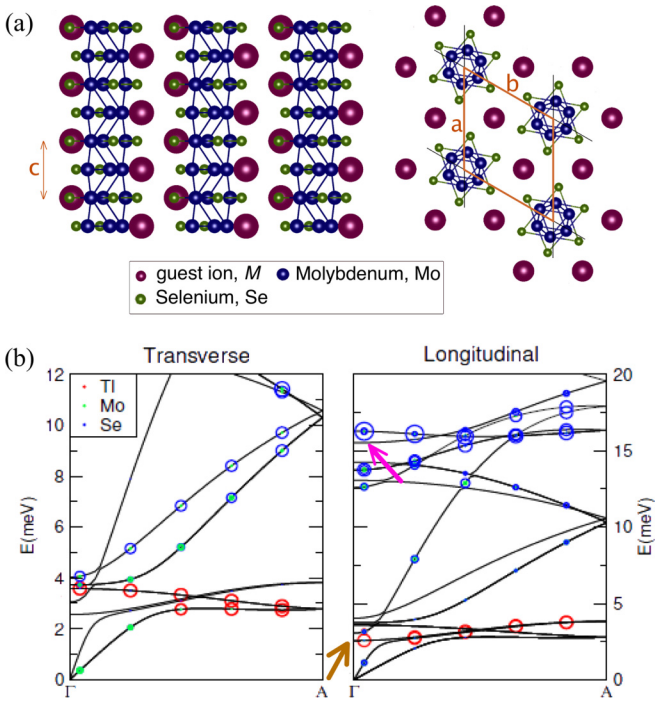

FIG. 1. (a) Crystal structure of $M_2Mo_6Se_6$, seen along a (left) and along the unique axis c (right). (b) Calculated phonon dispersions for $Tl_2Mo_6Se_6$. Colored circles mark the contributions from Tl, Mo, and Se for the transverse (left) and longitudinal (right) phonons. The longitudinal guest-ion and chain modes are marked by a brown and a purple arrow, respectively. Note the different energy scales for the two panels.

at temperatures $T_X \simeq 4$–5 K in $Tl_2Mo_6Se_6$ further supports the q1D nature of the electronic structure [18,19]. Nevertheless, an expected Peierls-like instability of the system [10,20] has not been found yet and the absence of a structural phase transition is remarkable given the highly nested Fermi surface.

The family members of $M_2Mo_6Se_6$ share structural similarities with the unconventional superconductors $K_2Cr_3As_3$ [21,22], $Rb_2Cr_3As_3$ [23] ($T_c = 6.1$ K and 4.8 K, respectively), and KCr_3As_3 [24] ($T_c = 5$ K), as well as with $TlFe_3Te_3$ [25] (ferromagnetic, no SC). These compounds have a different valence count and the compounds with 233 stoichiometry have a different arrangement of guest ions and may lack inversion symmetry, which is present in the 133 compounds $M_2Mo_6Se_6$, KCr_3As_3, and $TlFe_3Te_3$. The lattice dynamics of $K_2Cr_3As_3$ has been studied theoretically [26] and a few phonon modes of particularly strong coupling have been found. A Raman scattering study of $K_2Cr_3As_3$ found evidence for such EPC in the observation of Fano line shapes of the spectra but no temperature-dependent softening or peak splitting was observed [27].

In the heavy guest ion members of $M_2Mo_6Se_6$ with $M =$ Tl, In, and Rb the EPC of the low-lying vibrational modes have been previously analyzed with a combination of transport and specific heat measurements [7], which compares well to inelastic neutron scattering results on polycrystalline samples [28]. Rather sharp Einstein modes were found at low energy that related to the guest ion vibrations as identified by the scaling of their energy with the guest ion mass. For these low energy guest ion modes an anomalous difference of EPC between In and Tl compounds was identified and invoked to explain the difference in transition temperatures in $Tl_2Mo_6Se_6$ and $In_2Mo_6Se_6$ ($T_c = 4.2$ K and 2.85 K, respectively [7]). The SC coupling is, however, principally provided by higher energy modes of the metallic chains $(Mo_3Se_3)_\infty$, whose EPC has not yet been determined in fine detail [7].

In this paper, we report a study of the momentum resolved lattice dynamics, measured by inelastic x-ray scattering (IXS) as well as by Raman scattering. Two types of modes are of principal interest: the low energy guest ion modes and the higher energy Mo_3Se_3 chain modes. They are seen (for the example of $Tl_2Mo_6Se_6$) as bands in Fig. 1(b) between 2–5 meV for the guest ion modes (strongly depending on guest ion mass) and 12–18 meV for the chain modes (nearly independent of the guest ion). Typical eigenmodes of the two types of modes are shown as animated graphics in the Supplemental Material [29]. A survey across a large selection of family members allows us to identify guest ion and pure chain modes and verify with very high precision the scaling found previously [28]. We find a good agreement between calculations and experimental results, while deviations from the general trends are seen in $In_2Mo_6Se_6$. The lowering of the higher energy chain mode frequency in $In_2Mo_6Se_6$ contributes to explaining the large difference in superconducting transition temperature T_c.

This paper is structured as follows: The next section will describe experimental and numerical methods. Section III will summarize the findings that are discussed in Sec. IV, and the conclusions drawn from these are summarized in Sec. V.

II. METHODS

Needle-shaped samples with hexagonal cross section and thicknesses between 50 and 100 μm and up to 3 mm length were grown in sealed molybdenum or silica crucibles at temperatures between 1100 °C ($In_2Mo_6Se_6$) and 1700 °C ($Tl_2Mo_6Se_6$) by similar methods as described previously [5]. Details of the sample growth are given in the Supplemental Material [29].

IXS spectra were measured at beamline ID28 at the European Synchrotron Radiation Facility (ESRF) [30]. This instrument features a high resolution monochromator using a near-backscattering Si(9 9 9) Bragg reflection, a beam focusing system for a spot size of 60 × 200 μm (vertical × horizontal), and a multiplexing analyzer and detector system, again utilizing the Si(9 9 9) Bragg reflection. In this configuration the combined energy resolution is 3.2 meV. Part of the data were taken at higher energy resolution of 1.6 meV in the Si(11 11 11) configuration of the spectrometer. The resolution function of the spectrometer was measured in the same data acquisition campaign by scattering from amorphous acrylic glass. The samples were aligned in a Laue geometry with the c axis along the momentum transfer $\vec{Q}$. In this geometry the orientation of a^* and b^* axes (undetermined) is irrelevant and a phonon dispersion along c^* is measured for longitudinal phonons with eigenmodes along c. The data are analyzed by a numerical peak fitting that includes the central peak and pairs of phonon-related peaks at positive and negative energy transfer, weighted in intensity to the expected ratio at the given temperature ($T =$ 300 K). Raw spectra of IXS from $Tl_2Mo_6Se_6$ are shown in Fig. 2(a) as well as in the Supplemental Material [29].

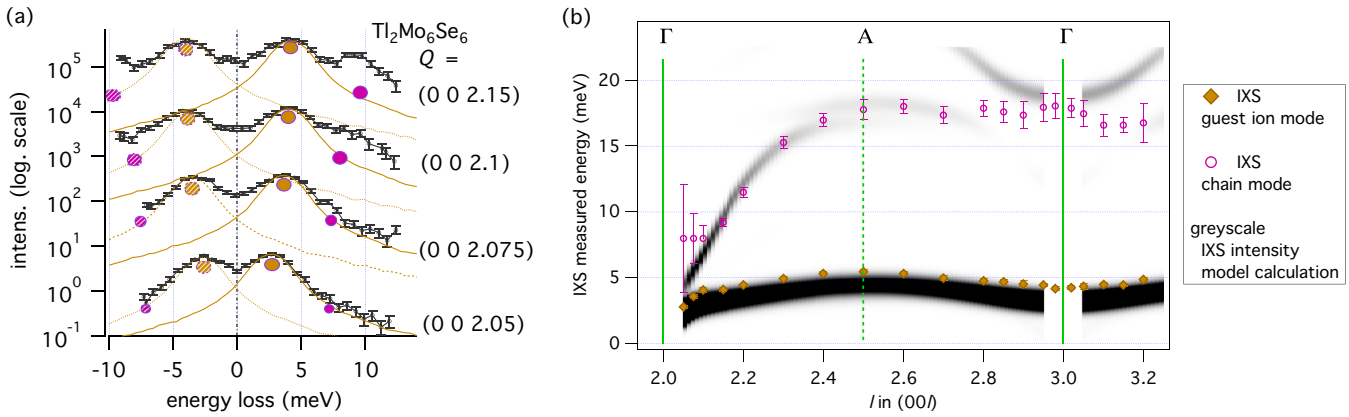

FIG. 2. (a) Selected IXS spectra of $Tl_2Mo_6Se_6$ close to the Γ point (002). Two observed modes are indicated by brown and purple color in solid symbols for positive energy loss and dashed symbols for negative energy loss. The resolution function, shifted to match the lowest, strongest phonon mode is shown in two copies in each spectrum. The spectra are offset vertically for graphical clarity. (b) Extracted phonon dispersions along the (00l) direction for longitudinal modes of $Tl_2Mo_6Se_6$. The data are overlaid on a grayscale representation of the expected IXS active modes in our scattering geometry. Error bars represent the statistical uncertainty of peak positions from the numerical fits applied to the raw spectra.

IXS dispersions $E(Q)$ were extracted from the spectra at each momentum point Q by numerical fitting of the raw spectra with a model consisting of shifted (along energy loss) and scaled (along intensity) copies of the measured resolution functions. For each phonon mode that is present in the spectra (one or two in the spectra of our study), a pair of resolution functions with energy losses $\pm E$ models the energy-loss and energy-gain features of the spectra. The relative intensities within these pairs take into account the detailed balance according to bosonic mode occupation at the known temperature (room temperature) and E. An additional scaled but unshifted resolution function is added to model quasielastic scattering. A fully summed spectrum of this kind is allowed to shift along the energy loss axis to compensate for small drifts of the zero point of the axis that can easily occur in IXS. The fit model thus has $2n + 2$ parameters, where n is the number of modes in the spectrum. The reported error bars are numerical uncertainties that derive from the fitting algorithm. An example of selected raw data is presented in Fig. 2(a) along with examples of resolution functions shifted in this manner for a single mode.

Raman scattering spectra were measured in a Renishaw inVia micro-Raman spectrometer equipped with a 632 nm laser. The laser beam was focused to an area of ≈3 μm and the power on the sample was kept below 2 mW. The scattered light was analyzed using a polarization filter before admission into the spectrometer. A box filter was used to suppress the intensity of elastically scattered light, which leads to a lowest analyzable phonon energy of 12 meV. The data from 20 subsequent detector exposures of 20 s dwell time were summed after removal of spurious intensities from the individual exposures.

Ab initio calculations of the lattice dynamics were performed within density functional perturbation theory (DFPT) [31], as implemented in QUANTUM ESPRESSO [32]. We employed nonrelativistic norm-conserving Martins-Troullier pseudopotentials [33], with nonlinear core corrections, from the standard QUANTUM ESPRESSO distribution, with a plane-wave cutoff of 80 Ryd; the exchange and correlation energy was treated in the generalized gradient approximation (GGA), in the Perdew-Burke-Ernzerhof parametrization [34].

For reciprocal space integration, we employed a $2 \times 2 \times 8$ regular grid in **k** space, and a Methfessel-Paxton smearing parameter of 0.02 Ryd; phonons were computed on a $2 \times 2 \times 4$ regular grid in reciprocal space, and dispersions on a finer mesh were then obtained by Fourier interpolation of the force constants. All calculations were carried out at the experimental lattice constants, reported in Ref. [7]. In order to have a more accurate estimate of the frequency of the soft phonon modes at the Γ point, the phonon frequencies were recomputed with all-electron LAPW calculations [35,36], with a much denser $(8 \times 8 \times 24)$ **k** grid and improved tetrahedron method [37], using the frozen-phonon approach. All calculated modes at Γ are listed in Table S1 in the Supplemental Material [29].

The calculated phonon dispersions along the c^* direction for $Tl_2Mo_6Se_6$ are shown in Fig. 1(b), where the left part highlights transverse modes (i.e., with eigenmodes orthogonal to c) and the right side highlights longitudinal modes. Modes with dominant contribution from one of the three ions of the compound are marked with colors.

III. RESULTS

We first report the results from the momentum-resolved IXS. Figure 2 shows the measured phonon dispersions for two modes up to $E = 25$ meV for $Tl_2Mo_6Se_6$. The momentum axis spans from $\vec{Q} = (0,0,2.0)$ to $(0,0,3.3)$. Only longitudinal modes contribute to the signal in this geometry. (002) is a strong Bragg reflection and corresponds to a Γ point, as does the Bragg-forbidden (003). The Brillouin zone boundary point A is reached at (0,0,2.5). The data are overlaid on a grayscale representation of predicted scattering intensities from the lattice dynamics calculation. The intensities were calculated by methods used in the ab2tds software [38].

At all probed momenta, the strongest IXS intensity from $Tl_2Mo_6Se_6$ arises from a mode with energies between 2.5–7 meV. This is a guest ion mode with similar but distinct eigenvectors on either side of the Brillouin zone boundary A, thus giving rise to different IXS intensities near (002) and near (003). From the strong Bragg spot (002) the steep dispersion of

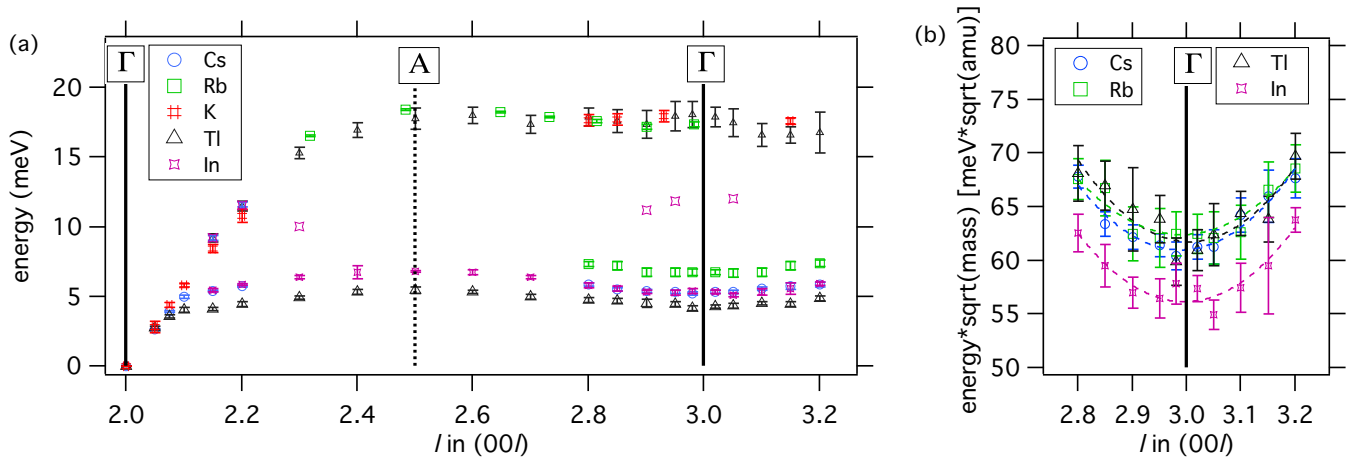

FIG. 3. (a) Longitudinal phonon dispersions for several $M_2Mo_6Se_6$. (b) A comparison of the dispersion of the guest-ion modes about the Γ point, normalized against the guest-ion mass.

the acoustic mode is observed, which bends into the flat guest ion mode. Near (003) and along the full length of $\ell = 2.5$–3, the guest ion mode is a nearly flat pure optical mode. The spectral features of this mode are sharp, resolution limited peaks, thus no sign of strong anharmonicity is observed.

A second peak at higher energy is found in the data between $E = 7$–17 meV. The comparison to the calculated IXS intensities shows that this is a well-defined single phonon mode only in small regions close to the Γ points. At intermediate momenta, namely around A, a superposition of intensities from related but separate phonon modes contributes to the intensity. Near (002) the steep dispersion bends into an optical mode of $E = 8$ meV (with large error bars), which shows that an avoided crossing is present to the acoustic branch of guest ion character. This is readily seen in the raw data of Fig. 2(a) as a double peak feature or excess scattering intensity beyond the strong lowest energy peaks. Near (003) the longitudinal mode can be identified and is indicated by an orange marker in Fig. 1(b). This is a nearly pure chain mode as shown below.

Figure 3(a) expands the results of Fig. 2(b) with data from a large number of different guest ions. As expected, the guest ion mode energies are different near (003), while the chain mode dispersion is identical for all measured family members within the error bars (±2 meV), thus proving its character without much guest ion involvement. For the lightest measured guest ion K, no guest ion mode could be detected. For the $In_2Mo_6Se_6$ sample, a few spurious extra peaks were detected in some of the spectra; these are marked by symbols without error bars.

The momentum region very close to the Γ point (003) is shown in Fig. 3(b). It is rare and fortunate to be able to measure IXS spectra so close to Γ as strong Bragg reflection intensity can dominate the spectra and preclude analysis. At (003) Bragg scattering is suppressed, which highlights the good quality of the crystals for all family members. Well-defined peaks with a clear dispersion are connected by parabolic fits to the data for each material. The data have been rescaled by division with the square root of the respective guest ion mass [39]. In agreement with earlier neutron scattering data [28] the mass-corrected phonon energies fall precisely on top of each other, both in terms of Γ-point energy as well as in terms of dispersion. This identifies the mode as a pure guest ion mode without any contribution of the chains. One exception is found in $In_2Mo_6Se_6$. Here the dispersion agrees with the other compounds, but the Γ-point energy is lower by 8%.

Raman scattering spectra are shown in Fig. 4(a) for compounds with five different guest ions. The lowest detectable Raman excitation was $E = 14$ meV in the range of chain modes; below this the necessary box filter removes the intensity. Data were measured with the polarization filter adjusted to either parallel to the crystal c axis (aligned by eye to the needlelike shaped sample) or orthogonal to it. The polarizations of incoming and outgoing photons were thus (c,c) or (a,a), respectively. While selection rules are not consistently giving rise to observed or suppressed peaks in all samples, the majority of peaks are visible only in (a,a) polarization. In this geometry, several rotational modes of Mo_3Se_3 triangles are expected to contribute to the Raman signal. The longitudinal modes that were observed in IXS are not Raman active.

We can now identify the Raman active modes with two methods. Purely experimentally we can verify the scaling with the guest ion mass; namely modes with identical energy for all family members are identified as pure chain modes. For $Tl_2Mo_6Se_6$ the comparison to the *ab initio* calculation further confirms this assignment. Figure 4(b) shows the analyzed peak positions for eight distinct peaks. In the range of 10–30 meV, we identify features #2, as well as #5 and #6 as mostly pure chain modes by their identical energies for K, Rb, and Cs. These modes are of E_{2u}, A_u, and E_{1g} symmetry with Mo/Se in-plane (#2 and #5) and out-of-plane (#6). Modes #1 and #3 show a trend of decreasing phonon energy with increasing guest ion mass across the series of alkali metals (K, Rb, Cs) and are identified as E_{2g} modes with Mo/Se out-of-plane and in-plane, respectively. Peak #1 may furthermore have a contribution from a Raman-active E_{1g} mode that is too close in energy to the E_{2g} to be resolved in the spectra.

IV. DISCUSSION

The data of a large number of members of the $M_2Mo_6Se_6$ family give a consistent picture of the lattice dynamics of both the guest ion and chain modes as well as collective modes. Specifically for $Tl_2Mo_6Se_6$, the observed data compare to

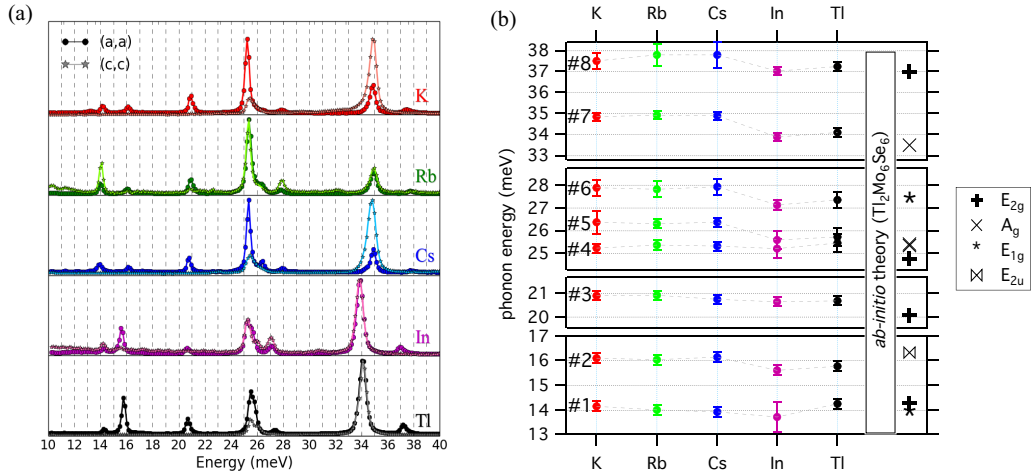

FIG. 4. (a) Raman spectroscopy of the low-energy phonon modes in the series $M_2Mo_6Se_6$. Spectra with the light polarization perpendicular and along the crystal c axis are shown as circles and stars, respectively. (b) Peak positions of all modes observed in (a) as a function of guest ion.

ab initio calculations with a good agreement. This agreement together with the resolution-limited peak widths and avoided crossings near Γ shows that none of the guest ion modes can be considered as rattling phonon modes. The lattice dynamics is truly collective at all momenta including the guest ion modes.

The rescaling to atomic masses of the guest ion, first reported in Ref. [28], is re-confirmed with much higher resolution thanks to being able to probe the longitudinal mode very close to $\Gamma = (003)$ in isolation. This confirms identical scaled phonon energies and thus a high purity of this guest ion mode. One exception is present in $In_2Mo_6Se_6$, which has a lower energy guest ion vibration. Previous studies did not have the resolution to find this difference in scaled mode energy but found a significantly weaker EPC for this mode in $In_2Mo_6Se_6$ when compared to $Tl_2Mo_6Se_6$ [7]. Surprisingly, our data show a softening of this mode in $In_2Mo_6Se_6$ when compared to the other family members, while a reduced EPC naively suggests that this mode should be hardened.

The chain modes, observed in Raman spectroscopy also show a deviation of $In_2Mo_6Se_6$ from the trends of the other family members. For several Raman active modes the phonon energies for $In_2Mo_6Se_6$ are significantly reduced when compared to the other family members. These chain modes provide most of the coupling responsible for SC [7] and their reduced energy leads to an effective reduction of the prefactor in the McMillan formula for superconductivity [40], partially explaining the reduced superconducting T_c. The actual difference in T_c between $Tl_2Mo_6Se_6$ and $In_2Mo_6Se_6$, which can be as high as a factor two, depending on samples, is however much larger than the observed softening, which is of the order of 5–10%; the remaining difference must come from a different coupling to the low-energy guest ion modes and/or to reduced matrix elements.

Also, $Tl_2Mo_6Se_6$ show slightly lower chain mode energies than expected from the trend across the whole series of Raman data. The measured energies are well reproduced by the calculation within 1 meV, with some modes higher and some lower than observed. Note that in all compounds the Raman peaks are sharp and show no visible sign of Fano line shapes at room temperature, thus these data do not provide direct evidence for a particularly strong EPC with no exceptions from material to material.

V. CONCLUSIONS

The data of IXS and Raman scattering, combined with the *ab initio* calculations for $Tl_2Mo_6Se_6$ give the consistent result that all members of the $M_2Mo_6Se_6$ series feature regular lattice dynamics as can be expected for compounds of this kind. The guest ion motion is harmonic and Einstein-like pure guest ion branches merge into collective modes with the expected anticrossing (observed in $Tl_2Mo_6Se_6$). Therefore, a rattling-mode description of the guest ions is not supported by the data. The data also show no indication of a soft mode that could be related to a Peierls-like phase transition, neither from the comparison of samples with varying interchain coupling nor by momentum dependent softening signatures in any given sample.

$In_2Mo_6Se_6$ falls out of the series because it exhibits both a reduced rescaled mode energy of the guest ion optical mode, when compared to the other family members, as well as reduced energies of several chain modes. $Tl_2Mo_6Se_6$ also has some reduced energies of these modes. This indicates that the difference between p-electron charge transfer for In and Tl, compared to s-shell transfer for alkali metals, influences not only the electronic interchain coupling [8] but also the bonding in the chains leading to softened chain modes. The stronger softening in $In_2Mo_6Se_6$ when compared to $Tl_2Mo_6Se_6$ partially explains the significantly lower superconducting T_c.

ACKNOWLEDGMENTS

We wish to thank O. K. Andersen and N. Ogita for fruitful discussions and A. Bosak and R. Burkovsky for technical assistance. Beamtime at beamline ID28 of the ESRF contributed to the results shown here. The Raman apparatus was provided by the Central Laser Facility of STFC. One of us (M.H.) would like to thank Hiroshima University and the Bodeleian Libraries for their kind hospitality during the time of writing this paper.

[1] P. Monceau, Adv. Phys. **61**, 325 (2012).

[2] T. Giamarchi, *Quantum Physics in One Dimension*, Vol. 121 of International Series of Monographs on Physics (Oxford Science Publications, Oxford, UK, 2003).

[3] F. J. Ribeiro, D. J. Roundy, and M. L. Cohen, Phys. Rev. B **65**, 153401 (2002).

[4] L. Gannon, A. Bosak, R. G. Burkovsky, G. Nisbet, A. P. Petrović, and M. Hoesch, Rev. Sci. Instrum. **86**, 103904 (2015).

[5] M. Potel, R. Chevrel, M. Sergent, J. Armici, M. Decroux, and Ø. Fischer, J. Solid State Chem. **35**, 286 (1980).

[6] R. Chevrel, P. Gougeon, M. Potel, and M. Sergent, J. Solid State Chem. **57**, 25 (1985).

[7] A. P. Petrović, R. Lortz, G. Santi, M. Decroux, H. Monnard, O. Fischer, L. Boeri, O. K. Andersen, J. Kortus, D. Salloum *et al.*, Phys. Rev. B **82**, 235128 (2010).

[8] A. Petrović, D. Ansermet, D. Chernyshov, M. Hoesch, D. Salloum, P. Gougeon, M. Potel, L. Boeri, and C. Panagopoulos, Nat. Commun. **7**, 12262 (2016).

[9] Q. D. Gibson, L. M. Schoop, L. Muechler, L. S. Xie, M. Hirschberger, N. P. Ong, R. Car, and R. J. Cava, Phys. Rev. B **91**, 205128 (2015).

[10] Q. Liu and A. Zunger, Phys. Rev. X **7**, 021019 (2017).

[11] S.-M. Huang, C.-H. Hsu, S.-Y. Xu, C.-C. Lee, S.-Y. Shiau, H. Lin, and A. Bansil, Phys. Rev. B **97**, 014510 (2018).

[12] J. Armici, M. Decroux, Ø. Fischer, M. Potel, R. Chevrel, and M. Sergent, Solid State Commun. **33**, 607 (1980).

[13] T. Mori, Y. Yokogawa, A. Kobayashi, Y. Sasaki, and H. Kobayashi, Solid State Commun. **49**, 249 (1984).

[14] Y. Tseng, G. Tessema, M. Skove, M. Potel, and P. Gougeon, Solid State Commun. **82**, 841 (1992).

[15] D. T. Verebelyi, J. E. Payne, G. X. Tessema, and E. Mengistu, MRS Proc. **478**, 157 (1997).

[16] J. Tarascon, F. DiSalvo, and J. Waszczak, Solid State Commun. **52**, 227 (1984).

[17] D. Ansermet, A. Petrović, S. He, D. Chernyshov, M. Hoesch, D. Salloum, P. Gougeon, M. Potel, L. Boeri, O. Andersen *et al.*, ACS Nano **10**, 515 (2016).

[18] S. Mitra, A. Petrović, D. Salloum, P. Gougeon, M. Potel, J.-X. Zhu, C. Panagopoulos, and E. E. M. Chia, arXiv:1710.00292.

[19] B. Bergk, A. P. Petrović, Z. Wang, Y. Wang, D. Salloum, P. Gougeon, M. Potel, and R. Lortz, New J. Phys. **13**, 103018 (2011).

[20] L. B. O.K. Andersen (private communication).

[21] J.-K. Bao, J.-Y. Liu, C.-W. Ma, Z.-H. Meng, Z.-T. Tang, Y.-L. Sun, H.-F. Zhai, H. Jiang, H. Bai, C.-M. Feng *et al.*, Phys. Rev. X **5**, 011013 (2015).

[22] T. Kong, S. L. Bud'ko, and P. C. Canfield, Phys. Rev. B **91**, 020507 (2015).

[23] Z. T. Tang, J. K. Bao, Y. Liu, Y. L. Sun, A. Ablimit, H. F. Zhai, H. Jiang, C. M. Feng, Z. A. Xu, and G. H. Cao, Phys. Rev. B **91**, 020506 (2015).

[24] Q.-G. Mu, B.-B. Ruan, B.-J. Pan, T. Liu, J. Yu, K. Zhao, G.-F. Chen, and Z.-A. Ren, Phys. Rev. B **96**, 140504 (2017).

[25] Z. Wang, X. Zhang, and S. Jia, J. Magn. Magn. Mat. **445**, 22 (2018).

[26] A. Subedi, Phys. Rev. B **92**, 174501 (2015).

[27] W.-L. Zhang, H. Li, D. Xia, H. W. Liu, Y.-G. Shi, J. L. Luo, J. Hu, P. Richard, and H. Ding, Phys. Rev. B **92**, 060502 (2015).

[28] R. Brusetti, A. J. Dianoux, P. Gougeon, M. Potel, E. Bonjour, and R. Calemczuk, Phys. Rev. B **41**, 6315 (1990).

[29] See Supplemental Material at http://link.aps.org/supplemental/10.1103/PhysRevB.98.014104 for animated graphics of typical Eigenmodes, raw data plots of IXS from $Tl_2Mo_6Se_6$ and $In_2Mo_6Se_6$ as well as a complete table of calculated mode energies and symmetries of $Tl_2Mo_6Se_6$.

[30] F. Sette and M. Krisch, *Inelastic X-ray Scattering from Collective Atom Dynamics*, Neutron and X-ray Spectroscopy, edited by F. Hippert, E. Geissler, J. L. Hodeau, E. Lelièvre-Berna, and J. R. Regnard (Springer, Dordrecht, NL, 2006).

[31] S. Baroni, S. de Gironcoli, A. Dal Corso, and P. Giannozzi, Rev. Mod. Phys. **73**, 515 (2001).

[32] P. Giannozzi, S. Baroni, N. Bonini, M. Calandra, R. Car, C. Cavazzoni, D. Ceresoli, G. L. Chiarotti, M. Cococcioni, I. Dabo *et al.*, J. Phys.: Condens. Matter **21**, 395502 (2009).

[33] N. Troullier and J. L. Martins, Phys. Rev. B **43**, 1993 (1991).

[34] J. P. Perdew, K. Burke, and M. Ernzerhof, Phys. Rev. Lett. **77**, 3865 (1996).

[35] O. K. Andersen, Phys. Rev. B **12**, 3060 (1975).

[36] P. Blaha, K. Schwarz, G. Madsen, D. Kvasnicka, and J. Luitz, *An Augmented Plane Wave Plus Local Orbitals Program for Calculating Crystal Properties* (Techn. Universität Wien, Austria, 2001).

[37] P. E. Blöchl, O. Jepsen, and O. K. Andersen, Phys. Rev. B **49**, 16223 (1994).

[38] See website, http://ftp.esrf.fr/scisoft/AB2TDS/.

[39] Data taken from webelements, https://www.webelements.com.

[40] W. L. McMillan, Phys. Rev. **167**, 331 (1968).